

In-Situ Characterization of Ni-Cu/SiO₂ Catalysts

T. S. CALE¹ AND J. T. RICHARDSON

Department of Chemical Engineering, University of Houston, Houston, Texas 77004

Received July 28, 1982; revised October 22, 1982

Novel equipment and analytical methods for *in-situ* magnetic, adsorptive, and kinetic analyses were developed primarily to characterize highly dispersed NiCu catalysts. Extended superparamagnetic superposition analysis provided direct evidence of composition heterogeneity in the Ni-Cu/SiO₂ samples studied. Hydrogen chemisorption and coupled magnetic-adsorptive experiments were consistent with mass balance limited surface enrichment in Cu. No definite mechanism selection was made, but phase separation is indicated.

INTRODUCTION

Multimetallic catalysts have received considerable attention, both industrially and for the correlation of physical and chemical properties with performance. The characterization of alloy systems will lead to more predictive, less expensive catalyst development. Several reviews in this area exist (1-4).

Nickel-copper is perhaps the most studied bimetallic system; though it plays no major industrial role, it was considered to be well suited for the testing of catalytic theory (1, 2, 5). Early inconsistent and surprising results were attributed largely to a theoretically predicted surface composition different from the overall, often referred to as surface-bulk heterogeneity (6, 7). The development of surface analytical methods over the last 20 years has aided our understanding of the causes and effects of surface-bulk heterogeneity (1, 3, 8, 9).

Phase separation, surface enrichment due to bond energetics, and chemically induced segregation can all contribute to surface-bulk heterogeneity in massive Ni-Cu samples (1, 2, 8-17). The last mentioned, though important, is not expected to influence this work (1, 8, 18). For samples equilibrated below the phase envelope (11,

19-22), both remaining effects need consideration (1, 8, 23). Samples quenched from as high as 1273K have shown copper enrichment in the surface, without phase separation (24, 25). A magnetic, adsorptive, and X-ray diffraction study on Ni-Cu powders, in this laboratory, also indicates surface enrichment without phase separation (26, 27). This agrees well with past results (28-30). A copper-enriched surface, somewhat dependent on history, is now accepted and has been shown repeatedly (1, 26). Modeling of these systems, an active area (8, 12, 13, 18, 31, 32), is improving our understanding.

Clustering in Ni-Cu has been observed, and is reasonable for endothermic alloys (33, 34). Surface clustering has also been predicted (35, 36) and would affect both physical properties and catalytic performance.

Relatively few characterization studies on supported Ni-Cu have been reported, and it is doubtful that the knowledge gained on massive samples is directly applicable to dispersed systems. For example, a suppression of the phase envelope has been debated (35, 37, 38), while enrichment should be enhanced by the lower coordination of surface atoms (31, 34). The increased dispersion also influences atomic diffusivities (39, 40), and raises the possibility of mass balance limited segregation (12, 31, 41).

¹ To whom correspondence should be addressed.





CASE	SCHEMATIC	PHASES	COMPOSITION
1		1	$x_2 < z \leq 1$
2a		2	$x_1 < z < x_2$
2b		"2"	$x_1 < z < x_1 + \Delta x$
3		1	$0 \leq z < x_1$

FIG. 1. The simple cherry model (1); z is nominal Cu fraction, x_2 is Cu in Cu-rich phase (~ 0.8), and x_1 is Cu in Ni-rich phase (~ 0.02). For dispersed systems Δx in case 2b can be large.

While a highly enriched surface can form at low copper content in massive samples, higher concentrations are required for highly dispersed samples. This is shown in Fig. 1, displaying the simple "cherry" model in phase separation (1). This aspect of highly dispersed bimetallics hampers interpretation, as the precipitous changes in physical and chemical properties with copper content, observed for massive samples, will be smoothed (see Fig. 2). Also, the difference between monolayer enrichment and phase separation becomes small.

Studies of supported Ni-Cu have generally utilized magnetic and/or adsorptive methods (1, 42). Robertson *et al.* (43), Dalmon (44), and Dalmon *et al.* (45) have studied silica-supported Ni-Cu in this way, while Maskos and van Hooff applied FMR to Ni-Cu on zeolite Y (46). From these studies, each crystallite is expected to have the same composition for reasonably uniform preparation methods.

The distribution of Ni and Cu in a crystallite is still unsettled. Dalmon *et al.* (44, 45) conclude intraparticle homogeneity, while data of Maskos and van Hooff (46) indicate heterogeneity. A pulsed adsorption study on Ni-Cu/SiO₂ (47) gave heat of adsorption and uptake results intermediate between those expected for homogeneous and segregated crystallites, and are consistent with mass balance limited segregation. A prelim-

inary high field (to 100 kOe) and adsorption study on Ni-Cu/SiO₂ in this laboratory indicates mass balance limited segregation (26). However, as in earlier work (44, 47), severe assumptions were required, and more direct analyses were desired.

This work was undertaken to develop *in-situ* methods to characterize supported Ni-Cu catalysts, and to study alloying effects on kinetics. Novel equipment and analyses for *in-situ* catalyst characterization were developed to determine intraparticle metal distribution and to interpret performance. Kinetic results are presented elsewhere (48). *In-situ* analyses were chosen for reliability, reproducibility, and ease of sample parameter adjustment. They avoid the difficult interpretations associated with analyses performed on different samples.

EXPERIMENTAL

Catalyst preparation. Ni-Cu/SiO₂ catalysts were prepared by homogeneous precipitation-deposition using urea (49). Details are given by Ginestra (47). The technique was developed to yield highly dispersed catalysts with uniform crystallite size (50). The final catalyst, Ni-Cu on Cab-O-Sil HS5 (300 m²/g), was crushed to pass

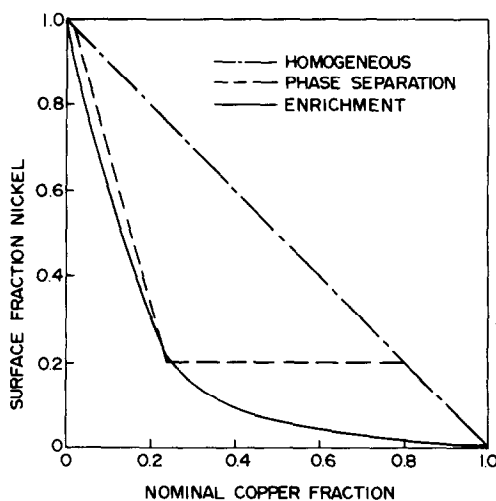


FIG. 2. The effect of high dispersion (0.25) on surface fraction Ni in phase separation and surface enrichment ($\Delta H_s/RT = 4(8)$).

TABLE I
Sample Compositions, Treatments, and Some Parameters of Interest

Sample	Percentage Cu ^a	Percentage metal	Weight (gm)	Treatment ^b	Time (hr)	w _m ^c (mg)	Area ^d (m ²)	R (nm)	Δ
1	0.0	22.9	0.393	A	8	70	7.7	2.18	0.37
2	0.0	22.9	0.524	A	12	98	10.2	1.94	0.35
3	0.0	22.9	0.522	B	12	111	13.6	2.18	0.39
4	0.0	22.9	0.522	C	1	112	13.3	2.20	0.39
5	2.6	25.1	0.415	A	9	73	7.4	1.91	0.30
6	2.6	25.1	0.525	A	10	84	7.8	1.92	0.41
7	2.6	25.1	0.520	B	14	96	10.3	2.13	0.38
8	6.0	25.3	0.463	A	8	80	6.7	1.89	0.37
9	6.0	25.3	0.544	B	17	88	7.7	2.06	0.37
10	6.0	25.3	0.544	B	19	89	7.6	2.01	0.42
11	12.0	27.9	0.493	A	12	70	4.6	1.92	0.38
12	12.0	27.9	0.551	B	12	88	6.9	2.04	0.44
13	12.0	27.9	0.551	B	13	87	6.9	2.06	0.45
14	21.1	27.1	0.490	A	11	75	3.8	2.35	0.43
15	21.1	27.1	0.530	B	12	69	4.3	1.99	0.35
16	21.1	27.1	0.530	C	1	69	4.4	2.02	0.43
17	31.1	27.2	0.484	A	11	47	2.1	1.88	0.44
18	31.1	27.2	0.562	B	20	52	2.9	1.74	0.45
19	39.8	21.6	0.528	A	12	34	1.8	1.50	0.30
20	39.8	21.6	0.528	A	16	36	1.6	1.54	0.33
21	39.8	21.6	0.527	B	34	38	2.0	1.80	0.49
22	39.8	21.6	0.527	C	1	38	2.2	1.80	0.48

^a Cu/(Cu + Ni) × 100.

^b A: Reduction at 673K, He cleaning at 723K; B: reduction at 723K, He cleaning at 783K; C: Heating at 783K under 10⁻⁶ Torr vacuum.

^c Assuming magnetism in Ni-Cu/SiO₂ samples results from a 98% Ni phase.

^d Hydrogen adsorption area.

100 mesh. Ni and Cu concentrations in Table 1 were determined colorimetrically and by X-ray fluorescence (26, 47).

Equipment. Complementary equipment, designed and fabricated for the special needs of this project, allows *in-situ* magnetic, adsorptive, and kinetic analyses. Details are given elsewhere (26, 51). It is *in situ* in that a sample is loaded in a cell, treated, kept under arbitrary conditions, and not perturbed until all analyses are completed.

***In-situ* sample cell.** Figure 3 shows a disassembled view of the flow sample cell with the catalyst sample in place. Flow is desired for sample treatments and kinetics. The body is quartz for inertness and operability over a large temperature range. A

quartz thermowell allows measurement of catalyst bed temperature. A high-vacuum Kontes valve and a high-vacuum Fischer-Porter valve, modified for in-line flow, allow vacuum to moderate pressure operation. In-line flow is required for the cell to pass through the magnetometer. Apiezon W is used to assemble the ground joints.

Sample cell operability has been shown for 77 to 1300K and 10⁻¹⁰ to 2 atm. The ends of the cell remain near room temperature to maintain vacuum-tight seals.

Magnetometer-cryostat. Figure 4 shows a cutaway view of the magnetometer-cryostat between the pole faces of the stabilized 15-kOe electromagnet. The fixed gap is 5 cm with 30.5-cm polepieces tapered to

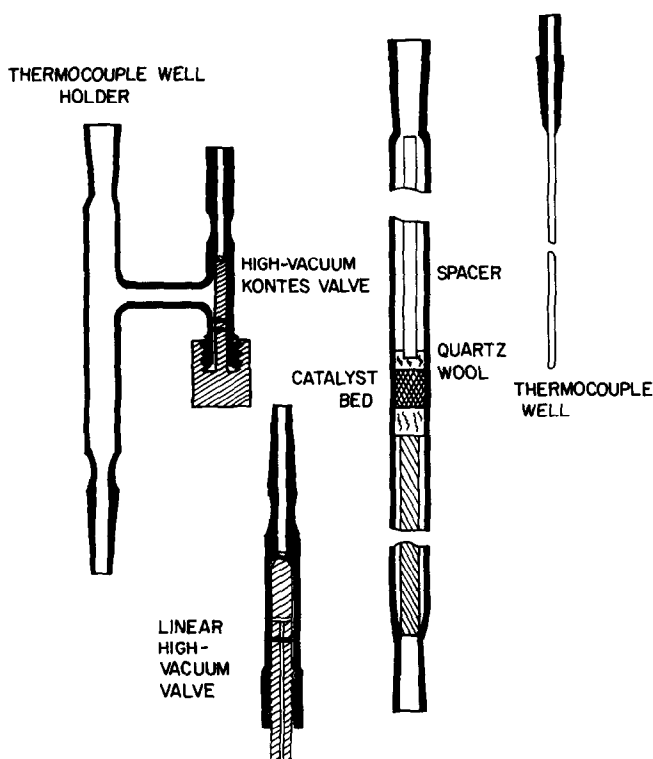


Fig. 3. Disassembled view of quartz sample cell with catalyst in place.

19-cm faces. Empirically, field uniformity is 0.1% over 7.5 cm of pole face.

The cryostat is fabricated from 316 stainless-steel sheet. The side port through the cryostat is used for field probe calibration. An o-ring union, soldered over the bottom port, serves to hold the central copper tube and seals the cryostat fluid. The cryostat temperature range is from 77 to 450K, with the magnetometer wire the limiting factor. A typical vacuum shield is 10^{-5} Torr.

The sample cell barely passes through the central copper tube, with the ends protruding to keep the seals at room temperature. The sample temperature, as measured in the thermocouple well, reaches within 0.1K of the liquid nitrogen bath, indicating the efficiency of indirect cooling. The magnetometer, mounted on the central copper tube, consists of two brass coil mounts of two coils each. Each mount is wrapped in series and then connected in a differential

mode for sensitivity and stability. The magnetometer is calibrated using bulk nickel standards, and response is linear with loading beyond any in this work. Sample lengths of 1.5 cm can be used without loss in signal. Sensitivity is such that magnetization equivalent to that of 0.01 g Ni can be studied with reliability.

Adsorption and kinetic equipment. Hydrogen chemisorption and kinetic experiments are performed on equipment designed to utilize the *in-situ* nature of the sample cell (26).

Chemisorption measurements are made on a glass volumetric apparatus. Attainable vacuum is 5×10^{-7} Torr, with a leak rate of less than 1 mTorr/hr. Manifold (61.2 cm³) pressure is measured with a differential capacitance manometer. This equipment is also used in sample treatment such as vacuum stripping and sintering.

A vacuum pump is connected to the ki-

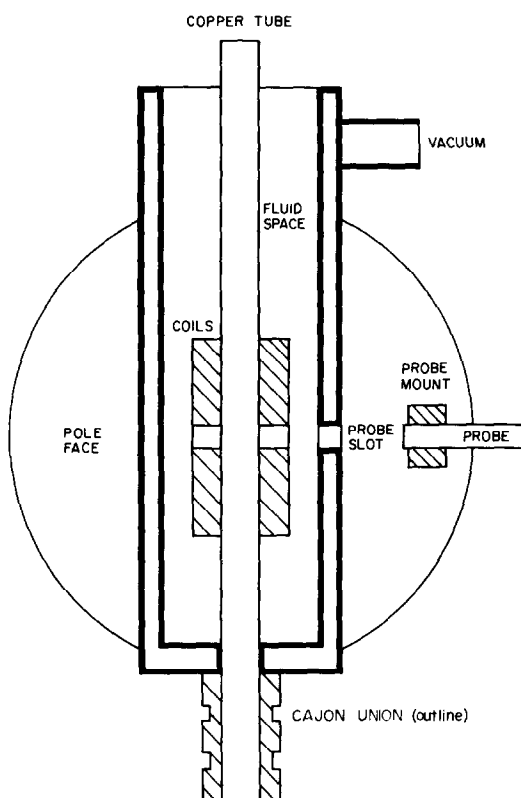


FIG. 4. Cross-section view of the magnetometer-cryostat between the magnet pole faces.

netic equipment upstream from the sample cell. After the cell is placed on the apparatus, the inlet lines are evacuated and purged to remove contaminants. Reproducibility of kinetic results is verification of success. This equipment is also used for catalyst reduction, cleaning, and sintering.

Experimental procedure. After the sample cell is loaded with about 0.5 g of catalyst, reduction is performed in flowing hydrogen (60 cm³/min) at temperature T_R . Cleaning, at 50K above T_R , is in flowing helium (90 cm³/min) or under vacuum on the adsorption manifold. The methods give the same results. High-purity (99.99%) hydrogen passes through an oxygen purifier, a silica gel trap, and a guard vessel (Ni/SiO₂ at $T_R + 50K$), and then over the catalyst sample. The 99.995% helium also passes through silica gel and guard catalyst before

contacting the sample. After reduction and cleaning, the sample is sealed under helium, or hydrogen for vacuum stripping, and removed from the equipment.

Adsorptive, magnetic, and kinetic analyses are now performed. A typical sequence is as follows. After alignment in the magnetometer-cryostat, a 300K magnetization isotherm is taken over 0–15 kOe. Liquid nitrogen is added to the cryostat, and after equilibration a 77K isotherm is recorded. The cell is then coupled to the adsorption unit. A 300K adsorption isotherm is taken from 0–300 Torr using ultrahigh-purity hydrogen (99.999%). After equilibration, sometimes requiring hours, the sample is removed for magnetic analyses under hydrogen.

Differential kinetic measurements, performed after the inlet lines are free of contaminants, can be made at this time. The sample is stored under hydrogen after performing kinetics. Magnetic analyses, as described above, are performed to check for changes in catalyst structure during reaction.

SUPERPOSITION ANALYSIS

Development

Determination of magnetic volume has been a primary difficulty in the study of magnetic bimetals, as moment density is unknown. Usually, severe reduction conditions are used and the assumption of complete reduction is made; however, this is still not a measure of magnetic volume. Superposition (52, 53) gives a method of estimating magnetic phase composition of superparamagnetic alloy specimens without knowledge of magnetic volume (26). Magnetic volume can then be estimated. The severe conditions needed for complete reduction are avoided, allowing flexibility in pretreatment conditions.

The relative magnetization of a collection of particles below a critical volume is (52)

$$\frac{M(H, T)}{M_{\infty}(T)} = \frac{M(H, T)}{I_s(T)V} = \int_0^{\infty} L(x)f(v)dv, \quad (1)$$

where

$$L(x) = \coth x - 1/x, \quad (2)$$

$$x = \frac{I_s(T)vH}{kT}, \quad (3)$$

I_s is spontaneous magnetization,
 M is total magnetic moment,
 H is applied field,
 k is Boltzmann's constant,
 T is thermodynamic temperature,
 V is total magnetic phase volume,
 v is magnetic particle volume,
 f is the particle size distribution,

and

$$\int_0^\infty f dv = 1. \quad (4)$$

This assumes that I_s and composition do not depend on crystallite volume. I_s is usually taken as that for the bulk material of the same composition (52).

For a given sample, $M(H,T)/I_s(T)$ is a function of $I_s(T)H/T$. This is the principle of superposition, generally used as a test of superparamagnetic behavior (52, 53). This is not useful if spontaneous magnetization is not known. More useful is a generalization of work by Abeledo and Selwood (54). Equation (1) is modified to

$$\frac{M(H,T)}{I_s(T)/I_s(T')} = I_s(T')V \int_0^\infty L \left[\frac{I_s(T)I_s(T')Hv}{I_s(T')kT} \right] f(v)dv, \quad (5)$$

where T' is any convenient reference temperature. If $\gamma(T,T') = I_s(T)/I_s(T')$, then Eq. (5) becomes

$$\frac{M(H,T)}{\gamma(T,T')} = I_s(T')V \int_0^\infty L \left[\frac{\gamma I_s(T')Hv}{kT} \right] f(v)dv. \quad (6)$$

This is a very useful equation, as $M(H,T)/\gamma(T,T')$ is a function of $\gamma(T,T')H/T$. By adjusting γ until magnetization isotherms at T and T' coincide, a reduced spontaneous magnetization (γ) vs temperature curve can

be generated (55–57). Specifically, $\gamma(77\text{K}, 300\text{K})$ is determined by adjustment until superposition of $M(H, 77\text{K})/\gamma$ vs $\gamma H/77\text{K}$ onto $M(H, 300\text{K})$ vs $H/300\text{K}$ (26). This is shown in Fig. 5.

The Langevin low-field approximation (52) is also useful, and can be used to show (as $H \rightarrow 0$) (26)

$$\gamma(T,T') = \frac{I_s(T)}{I_s(T')} = \left[\left(\frac{M}{H} \right)_T \left(\frac{H}{M} \right)_{T'} \frac{T'}{T} \right]^{1/2}. \quad (7)$$

This is easier to use than the trial and error adjustment above, but is more subject to error. Both methods lead to the same conclusions in this work.

Application

As noted, superposition can give a reduced magnetization–temperature profile. Profiles for bulk Ni and Ni–Cu alloys are available, and the shape is dependent on composition (55, 56). This can be used to estimate magnetic-phase composition, or attention can be limited to one pair of temperatures. Each composition will have a unique $\gamma(T,T')$, with resolution depending on T and T' (26). Figure 6 includes $\gamma(77\text{K}, 300\text{K})$ calculated from the data of Ahern *et al.* (55).

The composition of bulk alloys can be determined (1) by using the sample weight and saturation moment to determine I_s and hence composition, (2) by determining the Curie temperature, or (3) by determining γ as the ratio of saturation moments and determining composition from Fig. 6. This is shown for Ni and 15% Cu. Method (3) is more useful for supported material as the weight of the magnetic phase is not needed, and small crystallites do not have well-defined Curie points (52, 57). Complete reduction is easily achieved for powders, but not for supported Ni–Cu. Superposition analysis allows more flexibility in pretreatment.

This method has also been used to show a decrease in I_s with crystallite size for Ni/SiO₂ and Ni–Cu/SiO₂ (26, 57). Crystallite size distributions hamper determination of

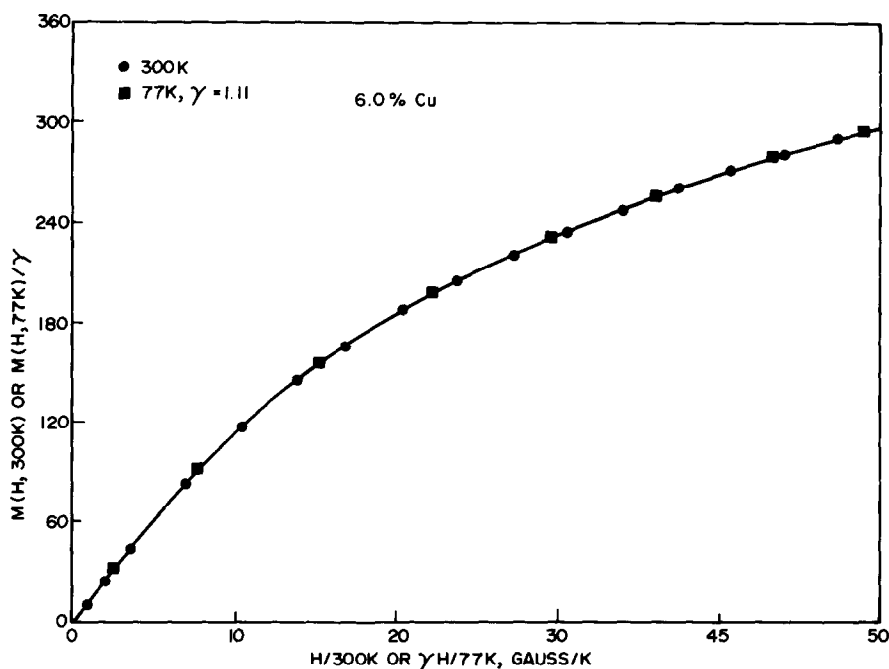


FIG. 5. Example of superposition analysis for a representative sample.

I_s as a function of size, but samples with Langevin low-field average radii much less than 3 nm display some effect (26, 57). Work is proceeding in this area. The samples in this study have close average size, so the effect is minimized and does not interfere with interpretation. A stronger effect at higher T/T_C (bulk Curie temperature)

has been shown (57). As will be seen, $T/T_C \leq 0.5$ for samples in this work, and I_s should be close to the bulk (26, 52). It is assumed that $I_s(77K)$ of a sample studied here is $I_s(77K)$ of a bulk sample, which is reasonable (57).

Another problem is deviation from superparamagnetism as crystallite sizes increase.

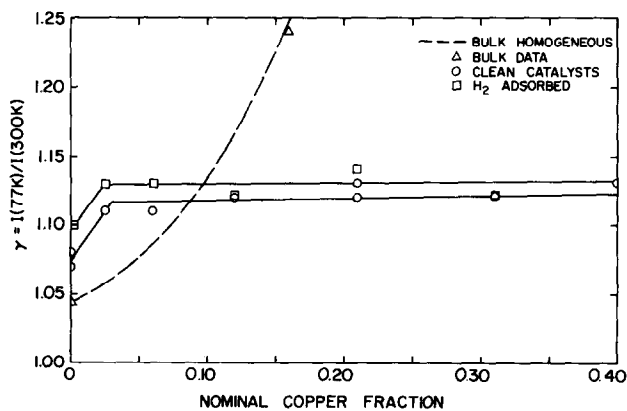


FIG. 6. Summary of superposition analysis. Included is the curve expected for homogeneous samples.

This occurs at low temperature first with deviation most noted at low fields (52). Experimentally, it was determined that 77 and 300K are reliable for samples with crystallites less than 4 nm in radius (26). For larger sizes, higher temperatures should be used.

RESULTS AND DISCUSSION

γ Results

Results of superposing entire magnetic isotherms are shown in Fig. 6; the same results were obtained using Eq. (7). The magnetic-phase composition is clearly independent of nominal copper content above a few percent, indicating heterogeneity with a high-nickel magnetic phase. Experimental reproducibility of γ is 0.01, and is small relative to the trend in Fig. 6.

The Ni/SiO₂ samples recorded have γ 's several percent high. This is attributed to size effects, as samples of larger size have the bulk γ (77K, 300K) (26, 57). Results after hydrogen adsorption, also shown in Fig. 6, demonstrate the effect of a magnetic dead layer on γ , as would be partially present if copper enriches the surface. These effects prevent a precise estimate of magnetic-phase composition, but the data indicate it to be less than 2.6% Cu. The composition used in this work is 98% Ni, consistent with past estimates (11, 21, 29).

These results are for samples of different history and percent reduction. The average crystallite sizes for the samples in Fig. 6 are near 2 nm. Ni-Cu/SiO₂ samples of larger crystallite size (around 3.5-nm radius) yield the same conclusions. No exhaustive effort was made to produce homogeneous crystallites; however, results on samples of varying reduction temperature (673 to 873K), cleaning (He vs vacuum stripping), and cooling (slow vs rapid cooling) did not alter the conclusion of heterogeneity (26).

This is the critical measurement of this work, since homogeneity is rejected for the samples studied. The mechanism of heterogeneity is not clear because of high dispersion, but the constancy of γ favors phase separation.

Crystallite Size and Reduced Metal

Heterogeneity complicates some matters considerably, as there is undetected material. Particle size and reduced metal are not directly determined for Ni-Cu/SiO₂ samples. A simple, cherry-like (1) model of a crystallite is used for tractability, a 98% Ni phase "inside" a copper-enriched layer (see Fig. 1). Magnetic material is assumed to have this composition; this is simplistic, but useful for calculation. For high-copper samples, several enriched layers may be necessary. Whether the surface is clustered or of uniform composition is not explicitly assumed. All crystallites in a sample are assumed to be the same shape and composition (43-46).

Referring to Fig. 1, magnetic reduced metal (w_m) and average magnetic crystallite size are less than the total reduced metal and average crystallite size. This is because of the nonmagnetic material present. If the fraction of total reduced metal which is magnetic is f , then reduced metal is w_m/f . The same correction is necessary for crystallite volume. Any effect of nonmagnetic material on magnetic estimates has been ignored. Extrapolation of high-field magnetization data at 77K is used to determine saturation and w_m (52). The crystallite sizes in these samples are large enough to make this a reliable approach, and reproducibility is within 1% (26).

Langevin low-field and high-field average volumes are used to characterize the size distribution (52). Parameters calculated from these are low- and high-field equivalent hemispherical radii (R_L and R_H), as well as (44)

$$R = \frac{R_L + R_H}{2} \quad (8)$$

and

$$\Delta = \frac{R_L - R_H}{R}. \quad (9)$$

This is the extent of size information needed, or justified, in this work. There is

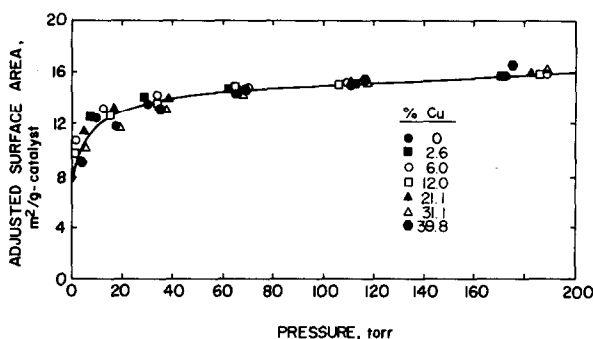


FIG. 7. Superposition of adsorption isotherms, after scaling, for representative samples at each composition.

no apparent trend in Δ with composition, and it averaged about 0.40 depending somewhat on sample history. This supports the assumption that each crystallite in a sample has the same composition, as differences should increase distribution breadth. For tractability in the remaining analyses, it will be assumed that each crystallite in a sample is the same size (e.g., R). R was adjusted to be large enough for reliable saturation estimates ($R_L > 1.5$ nm), but small enough to retain high dispersion and superparamagnetism at 77K.

The average radii between samples were also kept close to minimize dispersion differences and size effects on magnetic and kinetic properties. As seen in Table 1, most samples had $1.7 \text{ nm} < R < 2.2 \text{ nm}$. The actual radii ($R/f^{1/3}$) will tend to be closer together if there is a general decrease in R with increasing copper. This is critical, as in mass balance limited enrichment surface composition is a function of actual crystallite size. The same data were taken for hydrogen-covered catalysts with the expected trends (26).

Adsorption Results

Hydrogen chemisorption at 300K was used to estimate surface composition, as it is very selective to nickel (40). No significant amount of H_2 was adsorbed at 300K on a Cu/SiO_2 sample (26). It is assumed that $\text{H}:\text{Ni} = 1$ even at high Cu content (1, 58). Extrapolation to $p = 0$ of a line through the

high-pressure points was used to determine surface area (59). This is not critical, as an experimental, vertical scaling factor allowed fair superposition of isotherms, particularly at higher pressures. Figure 7 shows the typical coincidence for representative samples, implying that any consistent method will give the same trend.

Related to the surface fraction is the dispersion-adjusted specific hydrogen area ratio (44), denoted S . As mentioned, each crystallite in a sample is assumed to be the same in size and composition. If the average crystallite size for a Ni/SiO_2 and a $\text{Ni-Cu}/\text{SiO}_2$ sample is the same, no dispersion correction is necessary and

$$S = \frac{(\text{H}_2 \text{ area/crystallite})_{\text{NiCu}}}{(\text{H}_2 \text{ area/crystallite})_{\text{Ni}}} \quad (10)$$

H_2 area is the area determined as explained earlier, assuming only Ni adsorbs. The number of crystallites is determined directly from magnetic data as $(w_m/\rho)/\text{magnetic crystallite volume}$, if ρ is density. A reasonable dispersion correction for Eq. (10) is $\{R_{\text{Ni}}/(R_{\text{NiCu}}/f^{1/3})\}^2$ and S is determined if f is estimated.

Several methods can be used to correct for crystallite size. Comparing magnetic radii after H_2 adsorption is reliable if enrichment is confined to the surface layer, as is reasonable at lower copper content. Methods involving estimation of f are particularly useful as f is bounded between 1 and $w_m/\text{total metal}$ corresponding to minimum

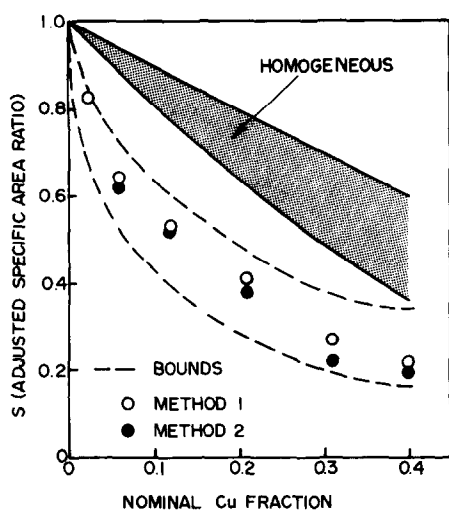


FIG. 8. Adsorption results showing extreme limits consistent with data and results after assumptions in text.

and maximum radius adjustment. These limits, consistent with the data, are the upper and lower dashed curves in Fig. 8. These are extremes, and more reasonable assumptions can be made. The points in Fig. 8 result from two of these: (1) the upper points result from assuming that the same proportion of Ni and Cu are reduced, and (2) the lower set results by assuming 100% reduction of Cu. Both methods additionally envision the formation of an 80% Cu phase for convenience. For clarity, each point is the average of several samples and the absolute reproducibility of S is 0.05 (26). The approaches are very different and employ radical assumptions, yet S is not affected much. As S is insensitive to method, the choice is not critical and probably lies between these two. More work is needed for better estimates of f .

The relation of S to surface fraction is usually considered to be between linear and quadratic, though neither can be considered satisfactory (1, 26, 44, 58). The shaded envelope in Fig. 8 shows the S expected for homogeneous crystallites, so adsorption results are consistent with mass balance limited segregation. Qualitative agreement with Fig. 2 is seen, with phase

separation showing better agreement at high copper content.

Magnetization-Chemisorption

The decrease in magnetization upon H₂ adsorption also gives information on the metal distribution in each crystallite. As heterogeneity hinders the interpretation of Selwood's ϵ (26, 44, 52), these numbers are reported as $\Delta M_{\infty}/H_2$ area in Fig. 9. Generally, ϵ is taken as the slope of the magnetization-volume isotherm, which is linear for H₂ on Ni/SiO₂ and Ni-Cu/SiO₂ up to relatively high pressure (44, 45, 52). In this work the change in magnetization was taken after the adsorption isotherm. This contributes somewhat to scatter, as only one point is used. The " ϵ " values obtained for Ni/SiO₂ average 0.76, while those obtained from magnetization-volume isotherms average 0.73 in this laboratory (26). This is in good agreement with past work (52).

The results in Fig. 9, where a linear S vs surface fraction is assumed, are consistent with mass balance limited segregation. Dalmon *et al.* (44, 45) conclude homogeneity since Ni-Cu surfaces remained magnetic. However, the magnetic moment of a Ni atom depends on the local concentration

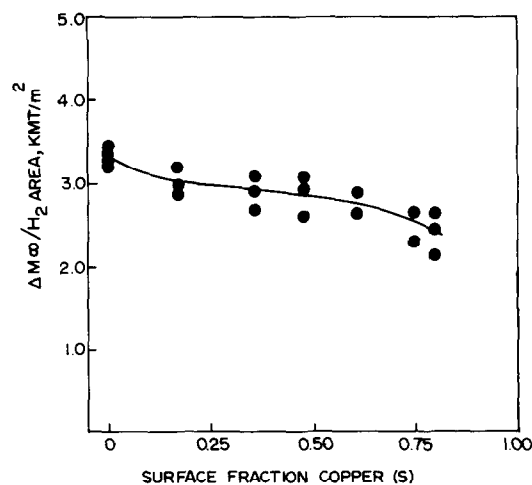


FIG. 9. Decrease in magnetization upon H₂ chemisorption assuming S is surface fraction.

(33). Results should be interpreted in terms of several outer shells, not just the surface. An enriched surface surrounding a 98% Ni phase should retain a majority of its magnetism, particularly if any clustering is present (26, 33). The initial decrease is attributed to the formation of a 98% Ni phase, rather than a pure nickel core. As multi-layer enrichment becomes reasonable, at higher copper, $\Delta M_{\infty}/H_2$ area begins to decrease.

CONCLUSIONS

In-situ techniques, particularly applicable to highly dispersed systems, were developed to characterize Ni-Cu/SiO₂. Superposition analysis provides direct evidence for heterogeneity. The constancy of the magnetic-phase composition indicates phase separation. Adsorptive and coupled adsorptive-magnetic analyses also indicate mass balance limited surface enrichment by copper. This is contrary to interpretations by Dalmon *et al.* (44, 45), but is consistent with other work (46, 47). High dispersion hinders mechanism selection as surface composition is determined by the amount of copper present, though phase separation is preferred.

The conclusion of enrichment in this study is not surprising in light of past work. Enrichment for bulk samples cannot be prevented by quenching, though phase separation can be (1). For highly dispersed systems, where segregation should be enhanced (8), enrichment is expected. Prevention of phase separation by quenching cannot be assumed for small crystallites, as atomic diffusivities are several orders of magnitude greater for these systems than for bulk catalysts at a given temperature (26, 40). It is estimated that quench rates comparable to those achieved with probe tips (10⁴C/sec) would be required to prevent redistribution (24). This would be difficult indeed for crystallites distributed in an insulating support. Thus enrichment by phase separation is not unreasonable, and

production of highly dispersed homogeneous crystallites may not be feasible.

The simple cherry-like model used is a good starting point; however, only qualitative consistency with experiment was achieved. This is expected considering its simplistic nature, and better agreement might occur with improved models. Further work on clustering, the effects of crystallite size distributions, and the possibility of adsorption-induced segregation is warranted. Accounting for crystallite size distributions is particularly important as surface composition is a function of nominal composition and size in mass balance limited segregation.

The characterization of dispersed Ni-Cu catalysts is needed to correlate catalytic patterns with electronic and/or geometric effects (1). Coupled characterization and cyclopropane hydrogenation-hydrogenolysis results indicate that both effects are important (48, 60).

ACKNOWLEDGMENTS

Financial support from the Robert A. Welch Foundation, the National Science Foundation, and Texaco is gratefully acknowledged.

REFERENCES

1. Sachtler, W. M. H., and van Santen, R. A., "Advances in Catalysis and Related Subjects," Vol. 26, p. 69. Academic Press, New York, 1977.
2. Ponc, V., *Catal. Rev. Sci. Eng.* **11**, (1), 1 (1975).
3. Moss, R. L., and Whalley, L., "Advances in Catalysis and Related Subjects," Vol. 22, p. 115. Academic Press, New York, 1975.
4. (a) Satterfield, C. N., "Heterogeneous Catalysis in Practice." McGraw-Hill, New York, 1980; (b) Gates, B. C., Katzer, J. R., and Schuit, G. C. A., "Chemistry of Catalytic Processes." McGraw-Hill, New York, 1979.
5. Dowden, D. A., and Reynolds, P., *Discuss. Faraday Soc.* **8**, 184 (1950).
6. Takeuchi, T., Tesuka, Y., and Takayasa, D., *J. Catal.* **14**, 126 (1969).
7. Takasu, Y., and Shimizu, H., *J. Catal.* **29**, 479 (1973).
8. In "Interfacial Segregation" (W. Johnson and J. Blakely, Eds.). American Society for Metals, 1979.
9. Ling, D. T., Lindau, I., Miller, J. N., and Spicer, W. E., Surface Composition of Cu-Ni alloys, *in*

- "Applied Surface Analysis" (T. Barr and L. Davis, Eds.), p. 66, ASTM STP 699. Amer. Soc. for Test. and Mater., 1980.
10. Ollis, D. F., *J. Catal.* **23**, 131 (1971).
 11. van der Plank, P., and Sachtler, W. M. H., *J. Catal.* **12**, 35 (1968).
 12. Williams, F. L., and Nason, D., *Surf. Sci.* **83**, 406 (1979).
 13. Overbury, S. H., Bertrand, P. A., and Somorjai, G. A., *Chem. Rev.* **75**, (5), 547 (1975).
 14. Abraham, F. F., Tsai, N., and Pound, G. M., *Surf. Sci.* **83**, 406 (1979).
 15. Bouwman, R., and Sachler, W. M. H., *J. Catal.* **19**, 127 (1971).
 16. Bouwman, R., Lippits, G. J. M., and Sachtler, W. M. H., *J. Catal.* **25**, 350 (1972).
 17. Harberts, J. C. M., Bourgonje, A. F., Stephan, J. J., and Ponec, V., *J. Catal.* **47**, 92 (1977).
 18. Tomanek, D., Mukherjee, S., Kumar, V., and Bennemann, K. H., *Surf. Sci.* **114**, 11 (1982).
 19. Rapp, R. A., and Maak, F., *Acta Met.* **10**, 62 (1962).
 20. Vecher, A. A., and Gerasimov, Ya. I., *Russ. J. Phys. Chem.* **37**, 254 (1963).
 21. Elford, L., Muller, F., and Kubaschowski, O., *Ber. Bunsenges. Phys. Chem.* **73**, 601 (1969).
 22. (a) Gates, B. C., Katzer, J. R., and Schuit, G. C. A., "Chemistry of Catalytic Processes." McGraw-Hill, New York, 1979; (b) Mozer, B., Keating, D. T., and Moss, S. C., *Phys. Rev.* **175**, (3), 868 (1968).
 23. (a) Sachtler, W. M. H., Dorgelo, G. J. H., and Jongepier, R., "Proc. Int. Symp. Basic Prob. Thin Film Phys., 1964," p. 218 (1965); (b) Sachtler, W. M. H., and Dorgelo, G. J. H., *J. Catal.* **4**, 100 (1965); (c) Sachtler, W. M. H., and Dorgelo, G. J. H., *J. Catal.* **4**, 654 (1965); (d) Sachtler, W. M. H., and Jongepier, R., *J. Catal.* **4**, 666 (1965).
 24. Ng, Y. S., McLane, S. B., and Tsong, T. T., *J. Vac. Sci. Technol.* **17** (1), 154 (1980).
 25. Ng, Y. S., Tsong, T. T., and McLane, S. B., *Surf. Sci.* **84**, 31 (1979).
 26. Cale, T. S., Ph.D. dissertation, Univ. of Houston (1980).
 27. Robb, W., M.S. thesis, Univ. of Houston (1975).
 28. Sinfelt, J. H., Carter, J. L., and Yates, D. J. C., *J. Catal.* **24**, 283 (1972).
 29. van der Plank, P., and Sachtler, W. M. H., *J. Catal.* **1**, 300 (1967).
 30. Cadenhead, D. A., and Wagner, N. J., *J. Catal.* **27**, 475 (1972).
 31. Kelley, M., *J. Catal.* **57**, 113 (1979).
 32. Lee, Y. W., and Aaronson, H. I., *Surf. Sci.* **95**, 227 (1980).
 33. Vrijen, J., and Radelaar, S., *Phys. Rev. B* **17**, 409 (1978).
 34. Donnelly, R. G., and King, T. S., *Surf. Sci.* **74**, 89 (1978).
 35. Moran-Lopez, J. L., and Falicov, L. M., *Phys. Rev. B* **18** (6), 2549 (1978).
 36. Helms, C. R., *Surf. Sci.* **69**, 689 (1977).
 37. Ollis, D. F., *J. Catal.* **23**, 131 (1971).
 38. Hoffman, D. W., *J. Catal.* **27**, 374 (1972).
 39. Yu, K. Y., Ling, D. T., and Spicer, W. E., *J. Catal.* **44**, 373 (1976).
 40. Anderson, J. R., "Structure of Metallic Catalysts." Academic Press, New York, 1975.
 41. Anderson, J. H., Conn, P. J., and Brandenberger, S. G., *J. Catal.* **16**, 404 (1970).
 42. Ponec, V., *Surf. Sci.* **80**, 352 (1979).
 43. Robertson, S. D., Kloet, S. C., and Sachtler, W. M. H., *J. Catal.* **39**, 234 (1975).
 44. Dalmon, J. A., *J. Catal.* **60**, 325 (1979).
 45. Dalmon, J. A., Martin, G. A., and Imelik, B., "Proc. 2nd Int. Conf. Sol. Surf. (1974)," *Jap. J. Appl. Phys.*, Suppl. 2, Part 2 (1974).
 46. Maskos, Z., and van Hooff, J., *J. Catal.* **66**, 73 (1981).
 47. Ginestra, J., M.S. thesis, Univ. of Houston (1979).
 48. Richardson, J. T., and Cale, T. S., in preparation.
 49. van Dillen, J. A., Geus, J. W., Hermans, L. A. M., and van der Meijden, J., "Proc. Sixth Intern. Cong. on Catalysis," p. 677 (1976).
 50. Dubus, R., M.S. thesis, Univ. of Houston (1977).
 51. Cale, T. S., and Richardson, J. T., in preparation.
 52. Selwood, P. W., "Chemisorption and Magnetization." Academic Press, New York, 1975.
 53. Bean, C. P., and Livingston, J. D., *J. Appl. Phys. Suppl.* **30** (4), 120S (1959).
 54. Abeledo, C. R., and Selwood, P. W., *J. Appl. Phys.* **32**, 229S (1961).
 55. Ahern, S. A., Martin, M. J. C., and Sucksmith, W., *Proc. Roy. Soc. Ser. A* **248**, 145 (1958).
 56. Kittel, C., "Introduction to Solid State Physics." Wiley, New York, 1976.
 57. Cale, T. S., Richardson, J. T., and Ginestra, J., submitted.
 58. Takasu, Y., and Yamashina, T., "Proc. 2nd Int. Conf. Solid Surf. (1974)," *Jap. J. Appl. Phys.*, Suppl. 2, Part 2 (1974).
 59. (a) ASTM Method, in progress; (b) Anderson, J. R., "Structure of Metallic Catalysts." Academic Press, New York, 1975.
 60. Moran-Lopez, J. L., and Bennemann, K. H., *Surf. Sci.* **75**, 167 (1978).